# Vapor-liquid coexistence in many-body dissipative particle dynamics

P. B. Warren
*Unilever R&D Port Sunlight, Bebington, Wirral, CH63 3JW, United Kingdom*
(Received 4 June 2003; published 18 December 2003)

Many-body dissipative particle dynamics is constructed to exhibit vapor-liquid coexistence, with a sharp interface, and a vapor phase of vanishingly small density. The application to fluid mechanics problems involving free surfaces is illustrated by simulation of a pendant drop. The model is an unusual example of a soft-sphere liquid with a potential energy built out of local-density-dependent one-particle self-energies.

DOI: 10.1103/PhysRevE.68.066702 PACS number(s): 47.11.+j, 05.20.Jj

## I. INTRODUCTION

Dissipative particle dynamics (DPD) is familiar as a method of simulating complex fluids at a coarse grained level [1,2], for example block copolymer polymer melts [3,4], and surfactant solutions [5,6]. DPD has also been used for multiphase fluid problems, such as phase separation kinetics in binary liquid mixtures [7–9], droplet deformation and rupture in shear fields [10], and droplets on surfaces under the influence of shear fields [11]. The advantage of DPD for these kind of problems lies in the simplicity of the underlying algorithm, and the physical way in which singular events such as droplet rupture are captured. Such considerations also make the method attractive for *free-surface* fluid dynamics problems. Examples of these include various kinds of wetting, spreading, wicking, and capillary problems. To be used for these kind of problems, DPD needs to be extended to allow for vapor-liquid equilibrium. In this way a free surface will arise naturally as a vapor-liquid interface, and such an interface will possess the same physics as a clean vapor-liquid interface.

To achieve vapor-liquid coexistence in DPD, for a single-component system, requires a van der Waals loop in the equation of state (EOS) (pressure-density curve). However, this presents a fundamental limitation for standard DPD since the soft interaction forces used in the method invariably lead to a predominantly quadratic EOS [12]. One way around this is the ''many-body'' DPD method invented by Pagonabarraga and Frenkel [13,14] and also investigated by Trofimov *et al.* [15]. In many-body DPD, the amplitude of the soft repulsions is made to depend on the local density. In this way one can achieve a much wider range of possibilities for the EOS.

A similar approach to simulating liquid-vapor interfaces was introduced by Nugent and Posch in the context of smoothed particle applied mechanics (SPAM), also known as smoothed particle hydrodynamics (SPH) [16]. The connection between many-body DPD and SPAM and SPH has been greatly clarified recently by Español and Revenga [17], who introduce a ''smoothed DPD'' (SDPD) method as an SPH variant based on a new formalism developed for discrete hydrodynamics [18].

In the present work, many-body DPD is developed to exhibit vapor-liquid coexistence, with a sharp interface, and a vapor phase of vanishingly small density. The approach taken is fundamentally the same approach as used in Refs. [13] and [15], but with a somewhat different interpretation of the same mathematics. Therefore a general theory for many-body DPD is described first. It can be argued that this involves a fundamental reinterpretation of the DPD interaction potentials. The specific implementation for vapor-liquid equilibrium is described next, and finally the application to free-surface problems is illustrated by simulation of a pendant droplet. Another application to vapor-liquid phase separation kinetics was described in an earlier note [19].

## II. GENERAL THEORY

Dissipative particle dynamics is basically molecular dynamics [20,21], with two key innovations. The first, and perhaps the most profound, is the use of soft interactions. This stands in contrast to the common use of interaction potentials corresponding to particles with hard cores—for example, Lennard-Jones interactions or modified hard-sphere interactions. The second innovation is the use of a thermostat which conserves momentum locally. This allows one to simulate at a well-defined temperature yet preserve hydrodynamics, and this can be important for some problems such as phase separation kinetics. The thermostat described below is the original (Español-Warren) thermostat [22], although the Lowe-Andersen thermostat is perhaps simpler and more efficient [23]. In the present paper, the focus is on the equilibrium properties of many-body DPD models for which the nature of the thermostat is unimportant.

The particles in DPD have positions $\mathbf{r}_i$ and velocities $\mathbf{v}_i$, where $i=1-N$ runs over the set of particles, moving in a simulation box of volume $V$. They move according to the kinematic condition $d\mathbf{r}_i/dt=\mathbf{v}_i$ and Newton's second law $d\mathbf{v}_i/dt=\mathbf{F}_i/m_i$ where $m_i$ is the mass of the $i$th particle. Here

$$\mathbf{F}_i=\mathbf{F}_{i,\mathrm{ext}}+\sum_{j\neq i}\mathbf{F}_{ij} \tag{1}$$

is the total force acting on the $i$th particle, comprising a possible external force $\mathbf{F}_{i,\mathrm{ext}}$ and forces $\mathbf{F}_{ij}$ due to the interaction between the $i$th and $j$th particles. The interaction forces are decomposed into conservative, dissipative, and random contributions:

$$\mathbf{F}_{ij}=\mathbf{F}_{ij}^{\mathrm{C}}+\mathbf{F}_{ij}^{\mathrm{D}}+\mathbf{F}_{ij}^{\mathrm{R}}. \tag{2}$$

 ©2003 The American Physical Society

The individual contributions all vanish for particle separations larger than some cutoff interaction range $r_c$, and all obey Newton's third law so that $\mathbf{F}_{ij}+\mathbf{F}_{ji}=0$.

The conservative force is

$$\mathbf{F}_{ij}^{\mathrm{C}}=Aw_{\mathrm{C}}(r_{ij})\mathbf{e}_{ij}, \tag{3}$$

where $\mathbf{r}_{ij}=\mathbf{r}_j-\mathbf{r}_i$, $r_{ij}=|\mathbf{r}_{ij}|$, and $\mathbf{e}_{ij}=\mathbf{r}_{ij}/r_{ij}$. The weight function $w_{\mathrm{C}}(r)$ vanishes for $r>r_c$ and, for simplicity, is taken to decrease linearly with particle separation; thus $w_{\mathrm{C}}(r)=(1-r/r_c)$. The overall magnitude of the force law is determined by the amplitude $A$, which is the main parameter which is allowed to vary.

The force law in Eq. (3) corresponds to a total potential energy which is a sum of pair potentials:

$$U(\{\mathbf{r}_i\})=\sum_{j>i}\phi(r_{ij}), \tag{4}$$

where $-\phi'(r)=Aw_{\mathrm{C}}(r)$, and thus $\phi(r)=(A/2)(1-r/r_c)^2$ for standard DPD. The dissipative and random forces are $\mathbf{F}_{ij}^{\mathrm{D}}=-\gamma w_{\mathrm{D}}(r_{ij})(\mathbf{v}_{ij}\cdot\mathbf{e}_{ij})\mathbf{e}_{ij}$ and $\mathbf{F}_{ij}^{\mathrm{R}}=\sigma w_{\mathrm{R}}(r_{ij})\xi_{ij}\mathbf{e}_{ij}$. In these $\gamma$ and $\sigma$ are amplitudes, $w_{\mathrm{D}}(r)$ and $w_{\mathrm{R}}(r)$ are additional weight functions also vanishing for $r>r_c$, $\mathbf{v}_{ij}=\mathbf{v}_j-\mathbf{v}_i$, and $\xi_{ij}=\xi_{ji}$ is pairwise continuous white noise with $\langle\xi_{ij}(t)\rangle=0$ and $\langle\xi_{ij}(t)\xi_{kl}(t')\rangle=(\delta_{ik}\delta_{jl}+\delta_{il}\delta_{jk})\delta(t-t')$. The dissipative and random forces act as the above-mentioned thermostat provided that the weight functions and amplitudes are chosen to obey a fluctuation-dissipation theorem: $\sigma^2=2\gamma k_{\mathrm{B}}T$ and $w_{\mathrm{D}}=(w_{\mathrm{R}})^2$, where $k_{\mathrm{B}}T$ is the desired temperature in units of Boltzmann's constant $k_{\mathrm{B}}$ [22]. The same weight function is used as for the conservative forces (basically for historical reasons): $w_{\mathrm{R}}=w_{\mathrm{C}}$ and $w_{\mathrm{D}}=(w_{\mathrm{C}})^2$.

Usually all the particles are assumed to have the same mass, and to fix units of mass and length a convenient choice is to set $m_i=r_c=1$. Often the units of energy and hence time are fixed by setting $k_{\mathrm{B}}T=1$, but for equilibrium simulations it can be convenient to keep $k_{\mathrm{B}}T$ as a free parameter.

The integration of the equations of motion is a nontrivial matter since one has to accommodate the random forces. For an integration algorithm, Groot and Warren investigated a version of the velocity-Verlet scheme used in molecular dynamics simulations [2], but it was later shown by den Otter and Clarke that this is not a real improvement over a simple Euler-type integration scheme [24]. More extensive studies have been undertaken by Vattulainen *et al.* [25]. Alternatively, the Lowe-Andersen thermostat can be used, which is based on distinctly different physical ideas [23]. All the simulations described below were carried out with the simple velocity-Verlet-like algorithm described by Groot and Warren, with due care taken to avoid artifacts due to the finite size of the time step.

For a single-component DPD fluid, the equation of state gives the pressure $p$ as a function of the density $\rho=N/V$. For the soft potential given above, the EOS is now well established to be [2]

$$p=\rho k_{\mathrm{B}}T+\alpha A\rho^2, \tag{5}$$

where $\alpha=0.101\pm0.001$ is very close to the mean-field prediction $\alpha_{\mathrm{MF}}=\pi/30=0.1047$ (see also below). The first term in the EOS is an ideal gas term, and the second term is the excess pressure, which is almost perfectly quadratic in the density (there is a very small correction of order $\rho^3$). Note though that $\alpha A$ is *not* the second virial coefficient [12], so the above EOS is expected to break down for $\rho\lesssim1$. It seems that a quadratic EOS like this is unavoidable for soft potentials [12]. This represents the fundamental limitation to basic DPD mentioned in the Introduction. Moreover, one has to take force law amplitude in Eq. (3), $A\geqslant0$ (otherwise the pressure diverges negatively at high densities), so one is restricted to a strictly positive compressibility $\partial p/\partial\rho>0$. In fact, making $A<0$ throws the DPD pair potential into a formal class of catastrophic potentials for which it can be rigorously proved that there is no thermodynamic limit [12,26]. The situation is not as grim as it might seem though since considerable progress can be made for applications by introducing different species of particles and allowing them to be differentiated by their repulsion amplitudes; thus $A\rightarrow A_{ij}$ in Eqs. (3) and (4).

For the one-component fluid, an obvious way to get around the problem of a quadratic EOS is to make the amplitude $A$ in the force law dependent on density somehow. Such a scheme has been examined by several workers [13,15] and proves to be a simple extension to DPD. This many-body DPD requires only a modest additional computational cost, but throws open the possibility to simulate systems with an arbitrarily complicated EOS. The approach described here introduces a local density into the amplitude in the force law. By being explicit about the construction of the local density, this is a "safe" way to introduce a density dependence into the interactions [27,28].

In many-body DPD, the force laws are written as

$$\mathbf{F}_{ij}^{\mathrm{C}}=\frac{1}{2}[A(\overline{\rho}_i)+A(\overline{\rho}_j)]w_{\mathrm{C}}(r_{ij})\mathbf{e}_{ij}, \tag{6}$$

for a one-component fluid (Trofimov *et al.* [15] describe a multicomponent generalization). A partial amplitude $A(\overline{\rho})$ is introduced, depending on a weighted local density, which is defined for the $i$th particle to be

$$\overline{\rho}_i=\sum_{j\neq i}w_\rho(r_{ij}). \tag{7}$$

The weight function $w_\rho(r)$ vanishes for $r>r_c$ and for convenience is normalized so that $\int d^3\mathbf{r}w_\rho(r)=1$, although in principle the normalization could be absorbed into the definition of $A(\overline{\rho}_i)$. The discounted self-contribution $i=j$ in Eq. (7) would only add a constant $w_\rho(0)$ to $\overline{\rho}_i$, amounting to a constant shift of the argument in the definition of $A(\overline{\rho}_i)$ (see Trofimov *et al.* [15] for a more extensive discussion on this point). The weighted local density is readily computed by an additional sweep through the neighbor list; hence there is only a modest additional computational overhead. If $A(\overline{\rho})=A$, the method reduces exactly to the standard DPD model.

In mean-field theory, it is easy to show that the modified force law should give an EOS

$$p_{\mathrm{MF}}=\rho k_{\mathrm{B}}T+\alpha_{\mathrm{MF}}A(\rho)\rho^2, \tag{8}$$

where

$$\alpha_{\mathrm{MF}}=(2\pi/3)\int_0^\infty dr r^3 w_{\mathrm{C}}(r) \tag{9}$$

[i.e., $\alpha_{\mathrm{MF}}=\pi/30$ for the standard choice of $w_{\mathrm{C}}(r)$]. Thus, in principle, an arbitrary dependence on density can be recovered.

This is not the end of the story though. The existence of a potential energy $U(\{\mathbf{r}_i\})$ such that $\mathbf{F}_i=-\partial U/\partial \mathbf{r}_i$ requires the forces to obey a "Maxwell relation" of the type $\partial \mathbf{F}_i/\partial \mathbf{r}_j=\partial \mathbf{F}_j/\partial \mathbf{r}_i$. This is a nontrivial requirement since the particle positions appear both directly in Eq. (6) and indirectly through the definition of the local density in Eq. (7). One can show a necessary and sufficient condition for it to be true is that the derivative $w_\rho'$ is proportional to $w_{\mathrm{C}}$, so the two weight functions $w_\rho$ and $w_{\mathrm{C}}$ are not independent. One can then prove from the normalization condition on $w_\rho(r)$ that

$$-w_\rho'(r)=w_{\mathrm{C}}(r)/2\alpha_{\mathrm{MF}}, \tag{10}$$

where $\alpha_{\mathrm{MF}}$ is defined in Eq. (9).

What, then, is the corresponding potential? The answer is

$$U(\{\mathbf{r}_i\})=\sum_i u(\overline{\rho_i}), \tag{11}$$

where $u(\overline{\rho_i})$ is a self-energy depending on the local density, such that

$$u'(\overline{\rho})=\alpha_{\mathrm{MF}}A(\overline{\rho}). \tag{12}$$

Comparing Eq. (11) with Eq. (4), it is clear that there has been a *profound shift in perspective*, from a potential function expressed in terms of soft pair potentials, to one expressed in terms of density-dependent self energies.

There have recently been many discussions of the thermodynamic consistency of density-dependent interactions in the literature [27,29–31]. However, for the present formulation all thermodynamic relations are valid because the underlying potential $U(\{\mathbf{r}_i\})$ is a well-defined, density-independent function of the particle positions. This is important because it means for instance the virial equation for the pressure or stress tensor, constructed out of the forces, can be used without change.

If $u(\overline{\rho})$ is a polynomial in $\overline{\rho}$ of order $n$, it is easy to show that $\Sigma_i u(\overline{\rho_i})$ expands to a sum over $(n+1)$-body density-independent potentials. For $u(\overline{\rho})=\alpha_{\mathrm{MF}}A\overline{\rho}$, standard DPD is recovered.

It is worth emphasizing, contrary to some hints in the literature [13,15], that $\langle U(\{\mathbf{r}_i\})\rangle$ is the internal energy and *not* the excess free energy (here $\langle\cdots\rangle$ is a thermal average). It follows from Eqs. (8) and (11) that the mean-field EOS is $p_{\mathrm{MF}}=\rho k_{\mathrm{B}}T+\rho^2 u'(\rho)$. A standard thermodynamic result for the true pressure is $p=\rho k_{\mathrm{B}}T+\rho^2 f_N^{(\mathrm{ex})\prime}(\rho)$ where $f_N^{(\mathrm{ex})}(\rho)$ is the excess free energy per particle. This shows that the interpretation $u\equiv f_N^{(\mathrm{ex})}$ is a mean-field approximation and, as such, will be spoiled by correlation effects. Note also that correlations mean, typically, $\langle\overline{\rho_i}\rangle\neq\rho$, and $\langle u(\overline{\rho_i})\rangle\neq u(\langle\overline{\rho_i}\rangle)\neq u(\rho)$. Trofimov *et al.* give results for the mean local density and suggest ways that one might improve the correspondence between $\langle\overline{\rho_i}\rangle$ and $\rho$. Here a different approach is taken, in which $\overline{\rho_i}$ is regarded as a convenient intermediate quantity which is used to construct the forces; as such it is not important that its average differs from $\rho$. In practice, like Trofimov *et al.*, the mean-field EOS for many-body DPD can be considerably less accurate compared to standard DPD. Thus the method always requires calibration to determine the true thermodynamic properties (the approach of Trofimov *et al.* can be used to achieve a specific EOS).

## III. SPECIFIC MODEL

A specific application of these ideas to set up a DPD model which exhibits vapor-liquid coexistence is now described. Before this, though, there is one more technical point to discuss.

To stabilize the vapor-liquid interface, it is not sufficient just to have a van der Waals loop in the EOS; one must also give consideration to the ranges of the interactions. Thus simple many-body DPD with a single range may not have a stable interface as discussed by Pagonabarraga and Frenkel [13]. The trick employed here is to take the standard DPD model, make the soft pair potential attractive, and add on a repulsive many-body contribution with a *different* range $r_d<r_c$. Furthermore, the simplest form of the many-body repulsion is chosen. This is a self-energy per particle which is quadratic in the local density.

In terms of force laws, the standard DPD model as specified in Eq. (3) with $A<0$ is augmented by the addition of a many-body force law of the form

$$\mathbf{F}_{ij}^{\mathrm{C}}=B(\overline{\rho_i}+\overline{\rho_j})w_{\mathrm{C}}(r_{ij})\mathbf{e}_{ij}, \tag{13}$$

where $B>0$. This is Eq. (6) with $A(\overline{\rho})=2B\overline{\rho}$. The weight function in this is chosen to be $w_{\mathrm{C}}(r)=(1-r/r_d)$ for $r<r_d$. This means that $w_\rho(r)=15/(2\pi r_d^3)(1-r/r_d)^2$ (normalized for three dimensions) is used to construct the local density and $\alpha_{\mathrm{MF}}=\pi r_d^4/30$ for this particular interaction.

In terms of potentials, this model can be interpreted as follows. Define a generalized weight function of range $R$ via

$$w_\rho(r;R)=15/(2\pi R^3)(1-r/R)^2. \tag{14}$$

Then define *two* local densities $\overline{\rho}$ and $\overline{\overline{\rho}}$, constructed using this weight function with $R=r_c$ and $R=r_d$, respectively. The self-energy per particle for this specific model can be written as

$$u=(\pi/30)A\overline{\rho}+(\pi r_d^4/30)B\overline{\overline{\rho}}^2. \tag{15}$$

This is at most quadratic in the local densities, and thus the model could be written out explicitly in terms of two- and three-body interaction potentials. From this, the mean-field EOS is

$$p_{\mathrm{MF}}=\rho k_{\mathrm{B}}T+(\pi/30)(A+2Br_d^4\rho)\rho^2. \tag{16}$$

Thus, with $A<0$ and $B>0$, this EOS has the potential to contain a van der Waals loop. The actual EOS differs from this systematically, as will now be described.

## IV. SIMULATION RESULTS

The properties of the above model are now explored by simulation. First the actual EOS is examined, then vapor-liquid coexistence and the properties of a stable vapor-liquid interface are given, and finally we illustrate the potential application of the method with a simple pendant droplet simulation. Typical simulations presented here are in simulation boxes of size $10^3$ (units of $r_c$).

### A. Equation of state

For $B=0$ and $A>0$, the standard DPD model, the simulations recover the accepted EOS (5) with very small corrections of $\sim\rho^3$. Results are shown in Fig. 1(a).

For $A>0$ and $B>0$ a large number of simulations were performed. After some experimentation, the data were found to collapse to the following empirical EOS:

$$p=\rho k_{\mathrm{B}}T+\alpha A\rho^2+2\alpha Br_d^4\rho^2(\rho-c), \tag{17}$$

where $\alpha$ takes the same value as for standard DPD (and thus this expression contains the correct $B=0$ limit), and $c$ is an empirical correction to the density that appears in the many-body term. This should be compared to the mean-field prediction in Eq. (16). A representative sample of the data is shown in Fig. 1(b), where it is seen that Eq. (17) captures most of the systematic variation as $A$, $B$, $r_c$, and $\rho$ vary, provided $c$ is allowed to vary with $r_d$ as given in Table I.

For some parameter sets, the temperature was found to show strong deviations from the nominal $k_{\mathrm{B}}T=1$, as a result of instabilities in the integration algorithm. Results were only kept if the measured $k_{\mathrm{B}}T$ lay within 10% of the nominal value. These problems occur if the repulsion amplitudes are too large or the densities too high, or $r_d$ too small. The integration algorithm is that described in Groot and Warren [2], with a time step $\Delta t=0.05$ and $\lambda=1/2$. The instabilities can be vanquished by making $\Delta t$ smaller.

The measured equation of state is therefore quite close to the predicted mean-field equation of state. The main difference is a correction to the density dependence of the many-body term. This is expected since the pair correlation function $g(r)<1$ where the repulsions are strongest and thus $\langle\overline{\rho_i}\rangle<\rho$. This effect has also been checked in simulations by monitoring the mean value of the local density, with results similar to those reported by Trofimov *et al.* [15].

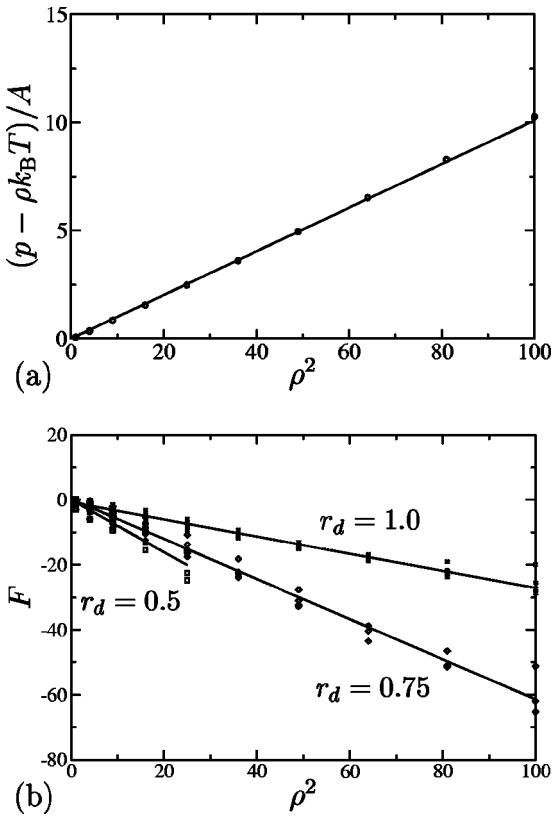


FIG. 1. Data collapse of pressure against density. (a) Standard DPD model, for $\rho=1-10$, $A=0-50$, and $k_{\mathrm{B}}T=1$. The straight line is a fit to data given by Eq. (5) in the text. (b) Many-body DPD model, for $\rho=1-10$, $A=0-50$, $Br_d^4=0-10$, $k_{\mathrm{B}}T=1$, and $r_d=0.5$ (squares), 0.75 (diamonds), and 1.0 (crosses). The ordinate is the function $F=(p-\rho k_{\mathrm{B}}T-\alpha A\rho^2-2\alpha Br_d^4\rho^3)/Br_d^4$. Plotted this way, the data collapse onto approximately straight lines, where the slope depends primarily on $r_d$. All quantities are expressed in DPD units.

### B. Vapor-liquid coexistence

For vapor-liquid coexistence, set $A<0$ and $B>0$ so that there is a van der Waals loop in the EOS. Phase separation is found in a range of densities $\rho_{\mathrm{V}}<\rho<\rho_{\mathrm{L}}$ where $\rho_{\mathrm{V}}$ and $\rho_{\mathrm{L}}$ are the vapor and liquid coexistence densities.

In principle, integration of the EOS gives the free-energy density from which predictions can be made about $\rho_{\mathrm{V}}$ and $\rho_{\mathrm{L}}$. Unfortunately, the EOS must deviate from the above fitted form for $\rho\ll 1$; therefore the vapor phase is inadequately characterized. For applications, one is most interested in $\rho_{\mathrm{L}}\gtrsim 1$ in coexistence with a very dilute vapor. If this is true, it is much easier to use the EOS to predict the point

TABLE I. Density correction "constant" for the many-body term in measured EOS, as a function of $r_d$. There is little significant dependence on other parameters $A$, $B$, and $\rho$ [see, e.g., Fig. 1(b)]. Figures in brackets are estimates of the error in the final digit.

| $r_d$ | 0.50 | 0.65 | 0.75 | 0.85 | 1.00 |
|---|---|---|---|---|---|
| $c$ | 4.0(5) | 4.1(1) | 3.07(5) | 2.08(5) | 1.29(5) |

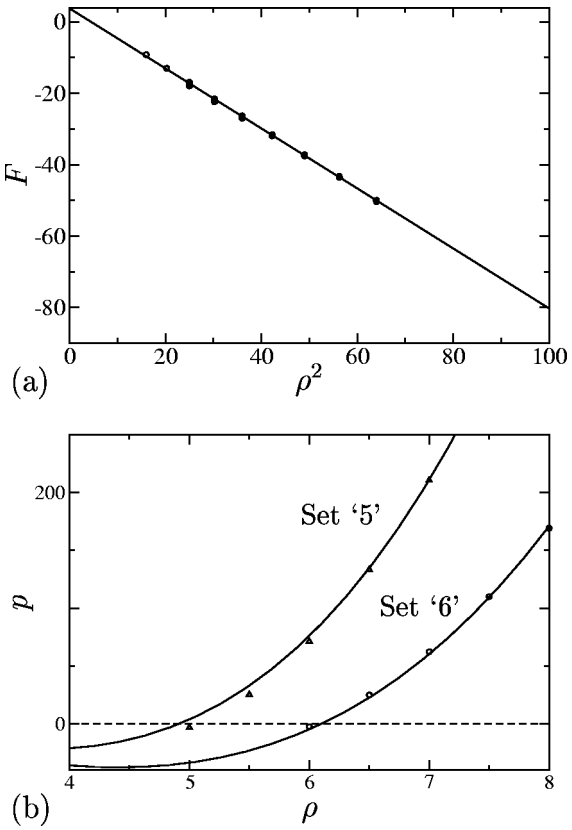


FIG. 2. (a) Data collapse of pressure against density, for $\rho_L < \rho \lesssim 8$, $A<0$, $|A|=20-40$, $B=25$ or 40, $k_BT=1$, and $r_d=0.75$. The ordinate is the function $F$ defined in the caption to Fig. 1. The straight line is a fit to data given by Eq. (18) in the text. (b) Pressure as a function of density for the two selected parameter sets in Table II. The lines are the predictions of the fitted EOS, Eq. (18) in the text. All quantities are expressed in DPD units.

where the pressure vanishes as an estimate of the coexisting liquid phase density. Thus $p(\rho_L)=0$. Using this, one expects liquid densities of the order $\rho_L \sim 5$ for $-A \sim B \sim 30$. From here on the range of the many-body repulsion is set to $r_d = 0.75$ as a midrange value determined above.

Since the above EOS was measured for $A>0$, one has to be careful to check that the scaling collapse still holds. One cannot easily measure the EOS within the phase separation region, since it is hard to maintain a stable uniform density. Therefore the EOS has been characterized for $\rho > \rho_L$. A similar data collapse is found to the previous section, as is shown in Fig. 2(a). In this case, the EOS can be fitted by

$$p = \rho k_B T + \alpha A \rho^2 + 2\alpha B r_d^4 (\rho^3 - c\rho^2 + d), \qquad (18)$$

where $\alpha = 0.101(1)$ as before, $c = 4.16(2)$, and $d = 18(1)$. The value of $c$ is similar to the value obtained previously [$c = 3.07(5)$, Table I]. There is an additional offset term $d$ which is about 10% of the density correction term $c\rho^2$ in the region of interest.

Although a wider parameter space was explored, two parameter sets were selected for more detailed work. These parameter sets are given in Table II (first three columns).

TABLE II. The two parameter sets used in subsequent simulations. The sets are distinguished by the different values of the liquid densities $\rho_L$. The coexisting vapor density $\rho_V \ll 1$, so these parameters are suitable for free-surface simulations. Also shown are the interface width $w$, surface tension $\sigma$, and compressibility at $\rho=\rho_L$ estimated from the EOS. All results are at $r_c = k_BT = 1$.

| Set | $A$ | $B$ | $r_d$ | $\rho_L$ | $w$ | $\sigma$ | $\partial p/\partial\rho$ |
|---|---|---|---|---|---|---|---|
| 5 | −40 | 40 | 0.75 | 5.08(1) | 0.78(5) | 4.95(3) | 49(2) |
| 6 | −40 | 25 | 0.75 | 6.05(1) | 0.66(3) | 7.45(4) | 47(2) |

Figure 2(b) shows the prediction of the EOS (18) compared directly against the measured pressures, for these two parameter sets.

For these two parameter sets, the coexisting vapor and liquid densities were determined from the vapor-liquid interface profile simulations described in the next section and are shown as a function of $k_BT$ in Fig. 3. Where $k_BT \neq 1$ in these simulations, the values of $A$ and $B$ are left at the values in Table II; in other words, $A$ and $B$ are regarded as absolute interaction energies. Also shown in Fig. 3 are the appropriate solutions of $p=0$ using the EOS (18).

It is clear that the difference $\rho_L - \rho_V$ gets smaller as $T$ increases, as one approaches the expected vapor-liquid critical point. At $k_BT \lesssim 1$, $\rho_V \ll 1$ indicating that the vapor phase is virtually devoid of particles. At $k_BT=1$ the solution to $p=0$ for the EOS gives a good estimate of the density of the fluid phase.

The EOS can also be used to estimate the compressibility $\partial p/\partial\rho$ at $\rho=\rho_L$, and the values are shown in Table II. Although the precise value is not important, the fact that $\partial p/\partial\rho \gg 1$ at the coexisting fluid density (where $p \approx 0$) shows that the fluid phase is relatively incompressible, similar to a real liquid.

### C. Vapor-liquid interface

Simulations of the vapor-liquid interface were undertaken by taking an equilibrated volume of fluid in a periodic box at

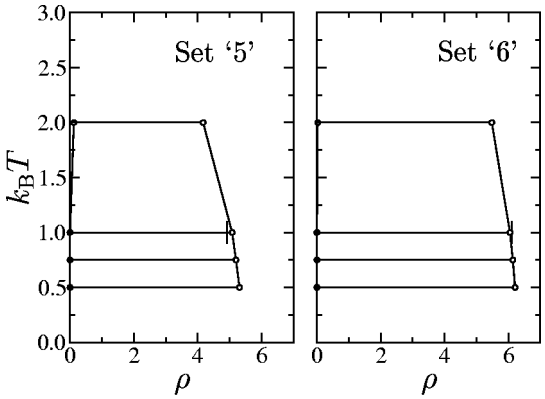


FIG. 3. Density-temperature phase diagrams for the two parameter sets in Table II, keeping $A$ and $B$ fixed. Shown horizontal are tie-lines computed from vapor-liquid interface profiles, at several temperatures (keeping $A$ and $B$ fixed). The short vertical line on the $k_BT=1$ tie-line is the point where the pressure vanishes according to the fitted EOS (18) in the text. All quantities are expressed in DPD units.

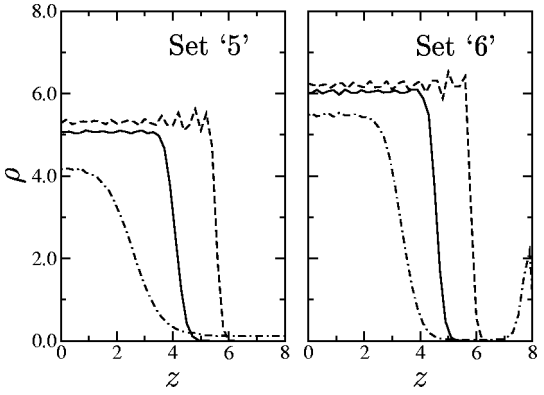


FIG. 4. Interfacial density profiles for the two parameter sets in Table II, for several values of the temperature (keeping $A$ and $B$ fixed): $k_BT=1$ (solid line), $k_BT=2$ (chained line), and $k_BT=0.5$ (dashed line). Distance through the interface is $z$. The zero of $z$ is arbitrarily chosen. All quantities are expressed in DPD units.

a density close to the $p=0$ limit and removing the particles in one-half of the box. The system was allowed to evolve until an equilibrium density profile was obtained. Interface profiles and surface tension values were measured as described for fluid-fluid interfaces [10]. For measurement of density profiles, it was necessary to stop the interface drifting over time. This was achieved by inserting a thin slab of ''frozen'' particles of thickness $r_c$ at one end of the box, where ''frozen'' means that the particle positions are fixed and the velocities are quenched to zero.

Figure 4 shows the interface profiles obtained this way for the two selected parameter sets in Table II. These are shown at several different values of $k_BT$ keeping $A$ and $B$ fixed. The limiting densities on either side of the interface were used to construct the tie-lines discussed in the previous section (Fig. 3). As the temperature is increased, the interfacial width $w$ gets broader, and the surface tension $\sigma$ drops. Results for $\sigma$ and $w$ are shown in Fig. 5. The width $w$ was quantified by calculating the maximum slope and normalizing to the coexistence densities, thus

$$w=\frac{\rho_L-\rho_V}{\max|d\rho/dz|}. \tag{19}$$

The surface tension is determined from the standard mechanical definition of the pressure tensor [20]. Note again that there is no problem with the many-body origin of the force laws. The actual forces enter the calculation in exactly the same way as standard DPD.

Low temperature favors a sharp interface, but if the temperature is too low, oscillations develop in the profile on the liquid side of the interface. This can be seen most clearly in Fig. 4 for $k_BT=0.5$. The system has crossed a Fisher-Widom line in the phase diagram, and a freezing transition is almost certainly nearby. The relative amplitude of the oscillations can be measured, and they are typically 10% of the bulk density at $k_BT=0.5$, but $<2\%$ for $k_BT\geqslant 0.75$, at least for the two sets of parameters studied here.

Thus the two parameter sets given in Table II provide for a sharp vapor-liquid interface, at $k_BT=1$, with virtually no

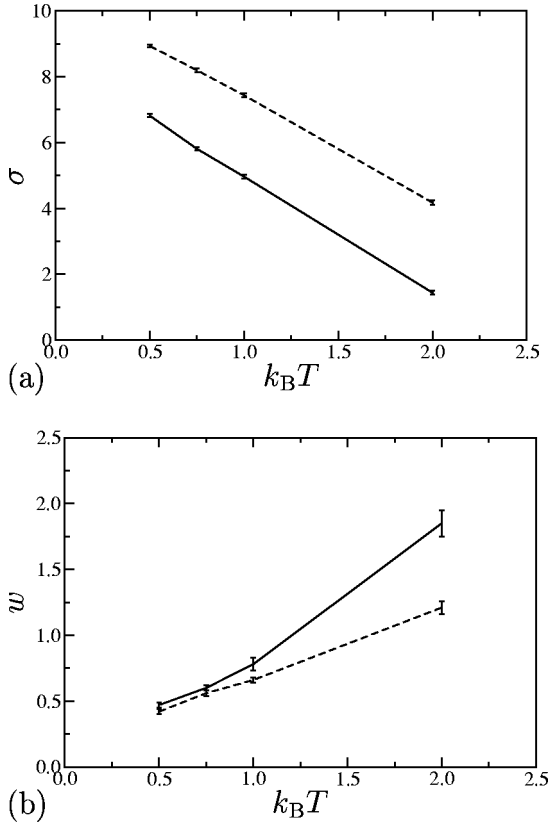


FIG. 5. (a) Interfacial tension $\sigma$ and (b) interface width $w$, as a function of temperature $k_BT$, for the two parameter sets in Table II (keeping $A$ and $B$ fixed): set 5 (solid lines) and set 6 (dashed lines). All quantities are expressed in DPD units.

particles in the vapor phase. They are thus well suited to model free surfaces. Table II also contains the measured interfacial properties.

### D. Pendant droplet simulation

As an example application, the classic pendant drop problem is now treated. The procedure is very similar to the one adopted for the DPD multiphase fluid model [10].

To set up the pendant droplet, a volume of fluid at a density close to the equilibrium liquid density was equilibrated, then replicated to construct a cylindrical column with the axis parallel to the $z$ direction. A ''support'' was constructed by ''freezing'' particles in a slice of thickness $2.5\,r_c$ at the top of the column so that their positions do not change and their velocities are quenched to zero. A gravitational body force $g$ was included by adding a constant force per particle directed along the $z$ direction away from the support. When the system reaches equilibrium, the liquid forms a pendant droplet suspended from the support particles. In equilibrium, the drop profile (radius as a function of height) was obtained as described below. The whole simulation takes a couple of minutes on a modern workstation. The droplet contains typically $\sim$3000 particles.

The profile was determined as follows. A $3d$ mesh was introduced with a resolution typically $\leqslant 0.5r_c$ (higher resolution was employed in the $z$ direction). The local particle

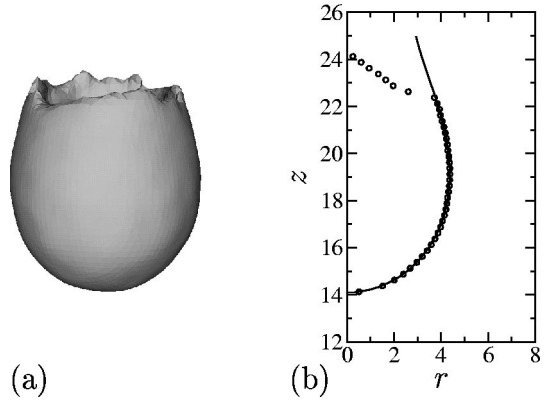


FIG. 6. Pendant droplet problem: (a) isosurface cut through $3d$ density field at $\rho=\rho_L/2$, showing the drop profile; and (b) drop radius $r$ as a function of height $z$, computed by the method described in the text. The zero of $z$ is arbitrarily chosen. The solid line is the Young-Laplace equation prediction; the circles are the measured profile. The ''frozen'' support particles at the top of the drop give a ragged edge to the top of the isosurface in (a) and distort the measured profile for $z \gtrsim 23$ in (b). Parameters correspond to set 6h in Table III. All distances are expressed in units of $r_c$.

density in each mesh volume element was computed by averaging over a period of time. This gives a $3d$ density field. The droplet can then be imaged as an isosurface or level cut through this density field, and a typical result is shown in Fig. 6(a).

To determine the drop radius as a function of height, the density field was divided (or ''segmented'') into occupied and unoccupied cells according to whether $\rho(\mathbf{r}) > \rho_L/2$ or not. The number of occupied cells at each height $z$ was used to compute the cross-sectional area of the droplet at that height and, therefore, the drop radius as a function of $z$. A typical drop profile is shown in Fig. 6(b).

This indirect procedure to determine the droplet radius eliminates two possible artifacts. First, it removes the blurring of the base of the drop by the interface profile, which would otherwise be $\sim(0.7-0.8)r_c$. Second, it eliminates effects due to the variation of fluid density with height which might otherwise introduce a systematic error if the mean particle number density as a function of height was computed directly. Such a variation of density with height is to be expected, since the fluid responds to the varying pressure field through the EOS (i.e., it is still a compressible fluid, even if only weakly so).

The drop profile was analyzed by normalizing with respect to the maximum diameter $\Delta E$ and comparing with a set of precalculated profiles as the Bond number $\beta=\rho_L g b^2/\sigma$ varies (where $b$ is the radius of curvature of the base of the droplet). The profiles are calculated from the Young-Laplace equation as described in earlier work [10]. From the best-fit $\beta$ value, the surface tension can be computed from $\sigma=\rho_L g \Delta E^2/H$ where $H(\beta)$ is a dimensionless function computed numerically.

Table III shows the quantities computed for several drops, for both parameter sets, and for several values of $g$. Although the surface tensions determined this way are not very precise, they are all consistent with the accurate values calculated directly from the interfacial profiles. The drop profiles all match the measured profiles quite accurately; see, for example, Fig. 6(b).

TABLE III. Pendant drop profile data. Interaction parameters are taken from Table II, according to the first digit of ''Set.'' The penultimate column is the surface tension computed from the drop shape, and the final column is the ''exact'' surface tension from Table II, computed by integration of the pressure tensor through a planar interface.

| Set | $g$ | $\rho_L$ | $\Delta E$ | $\beta$ | $1/H(\beta)$ | $\sigma_{\text{shape}}$ | $\sigma_{\text{exact}}$ |
|---|---|---|---|---|---|---|---|
| 5a | 0.022 | 5.08 | 8.80(5) | 0.378 | 0.57(3) | 4.9(3) | 4.95(3) |
| 6f | 0.025 | 6.05 | 9.00(5) | 0.378 | 0.57(3) | 7.0(5) | 7.45(4) |
| 6h | 0.033 | 6.05 | 8.75(5) | 0.404 | 0.52(2) | 7.9(4) | 7.45(4) |
| 6g | 0.030 | 6.05 | 8.70(5) | 0.431 | 0.48(4) | 6.6(5) | 7.45(4) |

## V. DISCUSSION

The model developed here can be discussed in several contexts. First, it is a new simulation method for fluid mechanics problems involving liquids with free surfaces. For example, the above pendant droplet problem is a test of the static force balance and the results show that the DPD fluid obeys the Young-Laplace equation in a nontrivial geometry. One can conclude that this particular version of many-body DPD offers a viable route for solving capillary problems such as the distribution of liquids in porous materials. It is clearly possible to address dynamic force balance situations too, but these will require further testing and parametrization, particularly for the notorious problem of contact line dynamics.

Second, now that vapor-liquid equilibrium is achieved for a basic soft sphere model, one can ''dress'' the liquid up in various ways such as making the liquid particles into polymers or model amphiphiles. In this way, new methods can be constructed to simulate complex fluids with an *implicit* solvent. These developments are the subject of ongoing investigations and will be reported separately.

In a third context though, the reinterpretation of many-body DPD as a fluid whose potential energy is built out of local-density-dependent one-particle self-energies is quite novel from the point of view of liquid-state theory. Most previous work has concentrated on fixed pair potentials with hard cores, and only minor attention has been paid to soft potentials or density-dependent pair potentials. The present work though goes some way beyond these existing ideas.

It has long been recognized that an arbitrary $U(\{\mathbf{r}_i\})$ can be expanded as a sum over density-independent one-body, two-body (pair potential), etc., terms. Normally the one-body terms, or self-energies, are harmless constants which can be discarded, and most of the phenomena observed for liquids can be captured by truncating the expansion at the pair potential level. If one allows the pieces in such an expansion to acquire a density dependence though, then the one-body self energy is no longer necessarily a constant, and it is no longer necessary to go to the pair potential level to see interesting

physics. Many-body DPD as described here is an example of precisely this.

The phase behavior of the present model is also potentially very interesting. By analogy with related soft-core systems such as the Gaussian core model [12,32] and models for polymers of various architectures [33,34], the particles in the original DPD model are expected to freeze into a variety of ordered phases at low temperatures and intermediate densities, with a reentrant fluid phase at high densities. The version of many-body DPD presented in this paper is constructed to have a significant vapor-liquid coexistence region, as shown in Fig. 3, but the low-temperature ordered phases are presumably still present, as indicated by the presence of oscillations in the liquid side of the vapor-liquid interface in Fig. 4. In such a case, the collision between the vapor-liquid transition and these ordered phases could prove to generate rather unusual phase behavior, and the low-temperature properties of many-body DPD models may well be worth further examination.

## ACKNOWLEDGMENT

I thank R. D. Groot for many discussions in the early stages of development of the many-body DPD model.

[1] P.J. Hoogerbrugge and J.M.V.A. Koelman, Europhys. Lett. **19**, 155 (1992).
[2] R.D. Groot and P.B. Warren, J. Chem. Phys. **107**, 4423 (1997).
[3] R.D. Groot and T.J. Madden, J. Chem. Phys. **108**, 8713 (1998).
[4] R.D. Groot, T.J. Madden, and D.J. Tildesley, J. Chem. Phys. **110**, 9739 (1999).
[5] S. Jury, P. Bladon, M. Cates, S. Krishna, M. Hagen, J.N. Ruddock, and P.B. Warren, Phys. Chem. Chem. Phys. **1**, 2051 (1999).
[6] P. Prinsen, P.B. Warren, and M.A.J. Michels, Phys. Rev. Lett. **89**, 148302 (2002).
[7] P.V. Coveney and K.E. Novik, Phys. Rev. E **54**, 5134 (1996).
[8] S.I. Jury, P. Bladon, S. Krishna, and M.E. Cates, Phys. Rev. E **59**, R2535 (1999).
[9] K.E. Novik and P.V. Coveney, Phys. Rev. E **61**, 435 (2000).
[10] A.T. Clark, M. Lal, J.N. Ruddock, and P.B. Warren, Langmuir **16**, 6342 (2000).
[11] J.L. Jones, M. Lal, J.N. Ruddock, and N. Spenley, Faraday Discuss. **112**, 129 (1999).
[12] A.A. Louis, P.G. Bolhuis, and J.-P. Hansen, Phys. Rev. E **62**, 7961 (2000).
[13] I. Pagonabarraga and D. Frenkel, J. Chem. Phys. **115**, 5015 (2001).
[14] The method was also invented independently by R. D. Groot.
[15] S.Y. Trofimov, E.L.F. Nies, and M.A.J. Michels, J. Chem. Phys. **117**, 9383 (2002).
[16] S. Nugent and H.A. Posch, Phys. Rev. E **62**, 4968 (2000).
[17] P. Español and M. Revenga, Phys. Rev. E **67**, 026705 (2003).
[18] P. Español, M. Serrano, and H.C. Öttinger, Phys. Rev. Lett. **83**, 4542 (1999).
[19] P.B. Warren, Phys. Rev. Lett. **87**, 225702 (2001).
[20] M. P. Allen and D. J. Tildesley, *Computer Simulation of Liquids* (Clarendon Press, Oxford, 1987).
[21] D. Frenkel and B. Smit, *Understanding Molecular Simulation* (Academic Press, San Diego, 1996).
[22] P. Español and P.B. Warren, Europhys. Lett. **30**, 191 (1995).
[23] C.P. Lowe, Europhys. Lett. **47**, 145 (1999).
[24] W.K. den Otter and J.H.R. Clarke, Europhys. Lett. **53**, 426 (2001).
[25] I. Vattulainen, M. Karttunen, G. Besold, and J.M. Polson, J. Chem. Phys. **116**, 3967 (2002).
[26] D. Ruelle, *Statistical Mechanics: Rigorous Results* (World Scientific, Singapore, 1999).
[27] A.A. Louis, J. Phys.: Condens. Matter **14**, 9187 (2002).
[28] N.G. Almarza, E. Lomba, G. Ruiz, and C.F. Tejero, Phys. Rev. Lett. **86**, 2038 (2001).
[29] F.H. Stillinger, H. Sakai, and S. Torquato, J. Chem. Phys. **117**, 288 (2002).
[30] C.F. Tejero, J. Phys.: Condens. Matter **15**, S395 (2003).
[31] C.F. Tejero and M. Baus, J. Chem. Phys. **118**, 892 (2003).
[32] F.H. Stillinger, J. Chem. Phys. **65**, 3968 (1976).
[33] M. Watzlawek, C.N. Likos, and H. Löwen, Phys. Rev. Lett. **82**, 5289 (1999).
[34] C.N. Likos, N. Hoffmann, H. Löwen, and A.A. Louis, J. Phys.: Condens. Matter **14**, 7681 (2002).